ORIGINAL ARTICLE

Calculation of Dose Perturbation in Radiotherapy of Head and Neck Tumors Due to the Presence of Dental Implants: A Monte Carlo Study

Morteza Hashemizadeh [1], Nasim Shams [2], Mansour Zabihzadeh [1, 3, 4*] (ID) , Masoud Jamali [5], Zeinab Sedaghat [1], Omid Azadbakht [6]

[1] Department of Medical Physics, School of Medicine, Ahvaz Jundishapur University of Medical Sciences, Ahvaz, Iran

[2] Department of Oral and Maxillofacial Radiology, School of Dentistry, Ahvaz Jundishapur University of Medical Sciences, Ahvaz, Iran

[3] Department of Clinical Oncology, School of Medicine, Golestan Hospital, Ahvaz Jundishapur University of Medical Sciences, Ahvaz, Iran

[4] Cancer Research Center, Ahvaz Jundishapur University of Medical Sciences, Ahvaz, Iran

[5] Radiation Oncologist, Technical Manager in Sarerm Hospital, Tehran, Iran

[6] Department of Radiology Technology, Behbahan Faculty of Medical Sciences, Behbahan, Iran

*Corresponding Author: Mansour Zabihzadeh
 Email: manzabih@gmail.com

Abstract

Purpose: The presence of a dental implant across the irradiation beam has the potential to perturb the dose distribution. In this study, the effect of different commercial dental implants on dose distribution was investigated in electron beam therapy.

Materials and Methods: The Varian 2100 C/D linear accelerator (Linac) head was modeled precisely with proper components for electron mode (6 and 9 MeV) by MCNPX 2.6.1 and was benchmarked according to the International Atomic Energy Agency (IAEA) protocol, TRS -398. Dose distribution was calculated for Six different implant materials, including Titanium, Titanium alloy, Zirconia (Y-TZP), Zirconium oxide, Alumina, and PolyetherEtherKetone (PEEK), and for Four different scenarios.

Results: The highest and lowest increasing doses occurred for Y-TZP (114.44% and 108.69% for 6 and 9 MeV, respectively) and PEEK (104.85% and 98.84% for 6 and 9 MeV, respectively) directly in front of the implant, respectively. By removing an implant from the jaw, an increasing dose was not seen, but an increasing dose occurred behind its depths in the bone region (31.81 %).

Conclusion: The amount of dose perturbation due to the dental implant's presence depends on the beam energy, mass density, and atomic numbers of implants. Maximum and minimum increased doses were estimated for Y-TZP and PEEK implants, respectively. Considering the correction factors due to the presence of high density and atomic number dental implants are essential to estimate the accurate dose delivery in radiotherapy with electron beams.

Keywords: Dental Implant; Dose Distribution; Electron Therapy; Monte Carlo Calculation; Radiotherapy; Head and Neck Tumors.

DOI: https://doi.org/10.18502/fbt.v11i4.16514

Frontiers in
BIOMEDICAL
TECHNOLOGIES

1. Introduction

In 2019, head and neck cancer accounted for nearly 3% of all diagnosed cases in the US [1]. Dental prostheses are common among patients over 50 who suffer from head and neck cancer. Radiotherapy, especially megavoltage electron therapy, is an integral part of head and neck tumor cancer treatment accompanied by surgery and/or chemotherapy used to treat the head and neck cancers. The presence of a dental implant in the treatment area and/or in its surrounding regions affects the dose distribution of radiotherapy [1-4]. Many dental implants are made of different materials such as metal, ceramic, and polymer materials used commercially in the market [3]. Dental implants made of titanium and its alloys are considered the best option for producing dental implants [5]. Zirconium dental implants have emerged as a potential substitute for titanium in recent years. Nonetheless, they are not yet commonly used in dental implantation procedures in clinics. The practicality and potential of Polyether Ether Ketone (PEEK) in producing restorations free of metal have been highlighted by recent research. This is particularly relevant for individuals with allergies and bruxism [5-7].

Scattering of radiation from high-density and high atomic number (Z) materials within the oral cavity can lead to complications in both soft and bone tissues. It is an essential factor in the head and neck Treatment Planning System (TPS) to estimate the absorbed dose distribution in radiotherapy [2, 8]. The presence of dental implants in the radiation treatment area may elevate the risk of mucosal complications, including osteoradionecrosis and mucositis, due to radiation scattering effects [7, 9]. Clinical manifestations of osteoradionecrosis may include pain, suppuration, exposed necrotic bone, pathological fracture, and orocutaneous fistula [10]. The mandible is more often affected than the maxilla because the bone density of the mandible is higher and its vascularity is relatively lower. In radiotherapy, the mandible often receives a more significant dose of radiation than the maxilla, contributing to the development of osteoradionecrosis [11, 12]. Multiple fields or removal implants from patients may be used to avoid the perturbation effect of dental implants on dose distribution and to minimize the scattered dose to the healthy tissue around the treatment volume. Nevertheless, implant removal is traumatic and yields the patient toothless [10].

A significant amount of scattered radiation is a common result when megavoltage electron beams encounter metal objects. In megavoltage electron or photon beams, the dose enhancement magnitude from these scattered radiations is dependent on the mass density and the atomic number of the irradiated mass [10]. The presence of metal implants near the tumor in Computed Tomography (CT) images can introduce artifacts that make it challenging to accurately outline the tumor and ensure optimal dose distribution during treatment planning. The accurate practical determination of the dose disturbance in the vicinity of the metal implant is difficult due to the high dose gradient, the need for a dosimeter with high resolution and sensitivity, and the fine-tuning for repeated experimental measurement. However, the Monte Carlo calculation method for calculating such small dose changes does not face such problems. MCNPX 2.6 code was used to calculate the impact of dental implant materials on dose distribution during head and neck radiotherapy using 6 and 9 MeV electron beams in this research. According to some research, electron beam therapy can be used for dose boost [13] and superficial tumors and carcinomas such as lips [14], parotid glands [15, 16], and skin tumors [14].

Due to the lack of precise and limited information on the dose perturbation caused by dental implants during electron therapy for maxillofacial tumors, this study aims to investigate the effect of dental implants and bone on the dose distribution during electron therapy for maxillofacial tumors by two different energies, 6 and 9 MeV, and the obtained results were systematically compared.

2. Materials and Methods

2.1. Monte Carlo Calculation

The Varian 2100C/D linear accelerator (Linac) head was modeled precisely with proper components for electron mode by MCNPX 2.6 Electron source, target, primary collimator, vacuum window, scattering foil, ionizing chamber, mirror, and secondary collimator were simulated as the main parts of Linac head (Figure 1a). 6 and 9 MeV electron beams were simulated for 10×10 cm^2 filed size and Source to Surface Distance (SSD) of 100 cm. The cut-off energy to transport the photon and electron beam was 0.01 and 0.1 MeV [17, 18], respectively. 2×10^9 particles were transported to reach a relative error better than 2%. The voxel size was set to $0.1 \times 0.1 \times 0.1$

cm^3 dimensions to calculate dose profile curves in 0.9 cm (in front of the bone) and 2.1 cm (behind the bone) depth along the z-axis. The cylinder voxels with a 0.5 cm radius and 0.1 cm height were used to calculate the Percentage Depth Dose (PDD).

Six common dental implant materials with 154 mm^3 volume (Figure 1b) were used in this study. The materials, chemical compositions, and densities (g/cm³) of these materials are given in Table 1. A most common dental crown material (Y-TZP) was used for all implants. The dimensions of all implants and crowns were considered

the same. Implants were modulated as cylinders with 0.35 cm diameter and 1.6 cm height (the lowest commercial implant sizes). Crowns were modulated as a cap on implants. The dimensions and appearance are given in Figure 1b. Each dental implant material was placed into a modulated bone with $6 \times 2 \times 1$ cm^3 sizes (Figure 1b). Due to the close resemblance of water to human body tissue, the water phantom was equivalented to the human body, and all these implants with crowns were placed into the bone located in a water phantom. Four different phantoms were modeled to calculate and evaluate the
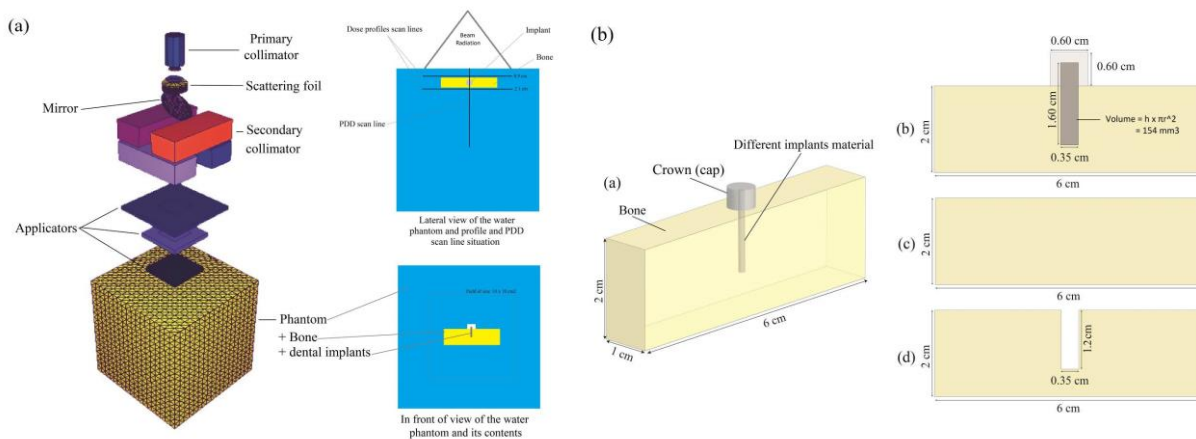

Figure 1. a. LINAC head elements and phantom simulation and in front of view of the water phantom and its contents and lateral view of the water phantom with dose profiles and PDD scan lines, b. (a) 3D view of the modeled bone with implant and crown, (b) Bone and implant, (c) Bulk bone, and (d) The bone that included the hole

Table 1. The common name, Chemical composition, and physical density of different implant materials

Materials	Common Name	Atomic Composition	molecular weight (amu)	Physical Density (g/cm^3)
Phantom	Water	H O	18	1.00
Titanium	Ti	Ti	47	4.54
Titanium alloy	Ti-6Al-4V	Ti Al V	407	4.34
Zirconia	Y-TZP	Zr Y O Al Si	350	6.01
Zirconium oxide	ZrO$_2$	Zr O	123	5.68
Alumina	Al$_2$O$_3$	Al O	100	3.97
Polyether ether ketone	PEEK	C H O F	288	1.3

dose distribution; a homogeneous phantom, a phantom with bulk bone, a phantom with bone that included the hole of retracted dental without the implant, and a phantom with bone and implant.

Additionally, YTZ-P and PEEK implants were selected for precise study. PDD curves and electron and photon fluences were calculated with high dose resolution in front of these implants by the cylinder voxel with a 0.5 cm radius and 0.01 cm height for 9 MeV. 2D dose profiles were calculated in front and behind both implants and bone for 6 and 9 MeV electron beams. In the Monte Carlo simulation and MCNP code, the utilization of variance reduction methods may produce results that are far from reality [19, 20]. Therefore, in this study, no variance reduction methods were used in MC calculations due to the need for high accuracy in the regions with high gradient doses (implant interfaces). All data were normalized to the maximum dose on the central axis in a water phantom for calculating PDD and dose profiles.

The Backscatter Factor (BSF) at the bone-implant interfaces, dose difference (ΔD), and implant volume were calculated by the following equations (Equations 1-3):

$$BSF = D_2/D_1 \quad (1)$$

$$\Delta D = D_2 - D_1 \quad (2)$$

$$Volume = h \times \pi r^2 \quad (3)$$

D_2 and D_1 are the doses with two different conditions. The h is the implant height and r is the implant radius.

2.2. Experimental Measurement

To confirm the accuracy of the MC modeled Varian Linac's head and adhere to the IAEA protocol TRS-398, measurements were taken of the PPDs and dose profiles of 6 and 9 MeV electron beams using a $0.13 \, cm^3$ Compact chamber (CC13, IBA company) in conjunction with the DOSE1 electrometer from Scanditronix-Wellhofer. These measurements were taken in an IBA-Blue water phantom from IBA dosimetry with a volume of $50 \, cm^3$ and then processed using RFAplus dosimetry software from Scanditronix-Wellhofer (Version 5.2).

3. Results

3.1. Benchmark Linac's Head

The electron beam that was used had an asymmetric Gaussian distribution and a FWHM right energy spectra of 2.5 and 2.2 MeV and a FWHM left energy spectra of 1.5 and 2 MeV [21, 22]. The tuning of the beam was done to achieve the best agreement between the MC calculations and measurements for beams of 6 and 9 MeV. Figure 2 shows the results for benchmarking the Linac's head for
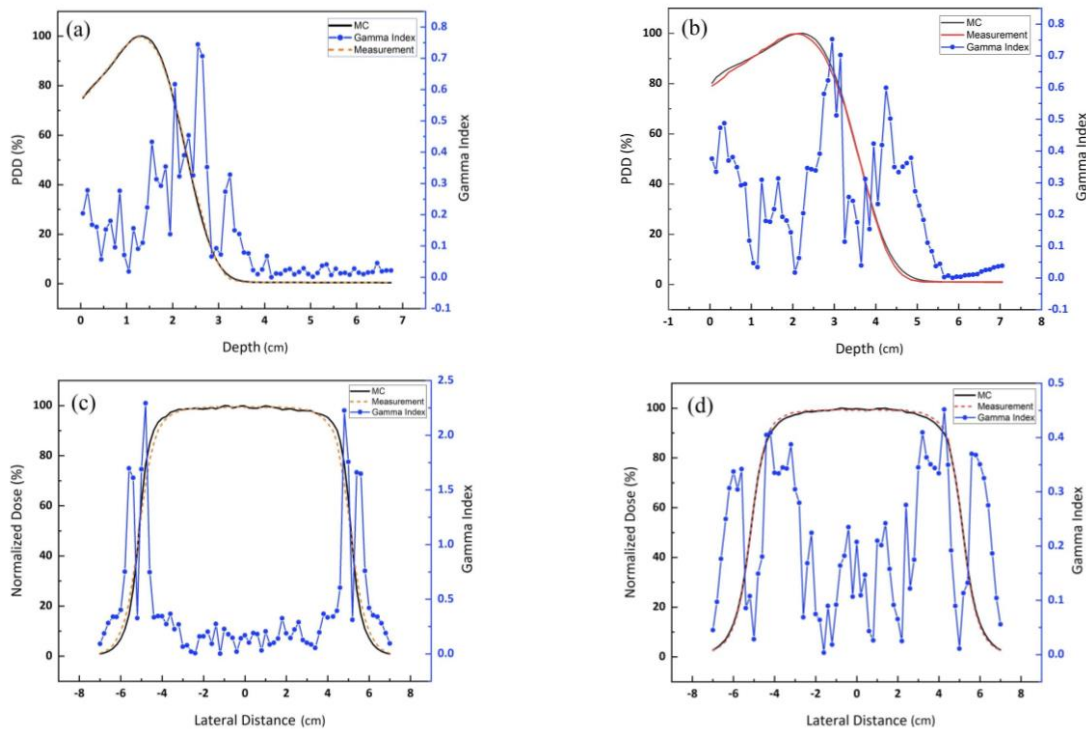

Figure 2. Comparison of calculated depth dose and dose profile curves with measurements in a homogeneous water phantom to benchmark the MC model. PDD and dose profile (depth of 10 cm) for 6 MeV (a. and c) and for 9 MeV (b., d.), respectively. The estimated gamma index (<1) shows that the measured data and the MC calculated are in good agreement

a field size of 10×10 cm^2 at a depth of R50 which the absorbed dose falls to 50% of the maximum dose. The estimated gamma index of (2%, 2 mm; < 1) confirms that the MC calculated and measured PDDs and dose profiles are in good agreement.

3.2. Calculated Dose Distribution at Different Regions and Scenarios

3.2.1. PDD Curves

Figure 3 shows the calculated PDD curves in 6 and 9 MeV electron beams for different scenarios; a homogeneous phantom, phantom with bulk bone, phantom with bone that included the hole of retracted dental without the implant, and phantom with bone and implant. All data in Figure 3 are normalized to the maximum dose of phantom without any inhomogeneity. Four regions in the phantom were controversial: in front and behind the bone (at a depth of 0.95 and 2.05 cm, respectively) and in front and behind the implant (at a depth of 1.25 and 1.75 cm, respectively). The quantity data of PDD for 6 and 9 MeV in these regions were collected in Table 2 and Table 3, respectively. Figure 4a shows the increasing total energy deposit effect in the bone area directly in front of the implant due to the presence of different materials (without phantom effect) for a 9 MeV electron beam. Figure 4b shows the electron and photon fluence in the bone area directly in front of the implant.

At 6 MeV, the soft tissue area located in front of the bone experienced the highest increase in dose when implant materials such as ZrO$_2$ and Y-TZP were used. The dose was found to be approximately 3.92% higher than that of the phantom without using any inhomogeneity and 1.79% higher than that of the bone (Table 2).
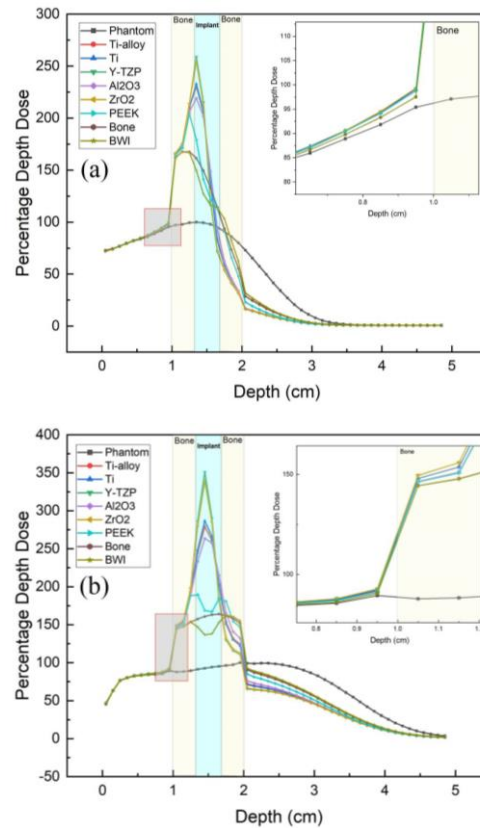

Figure 3. The percentage depth dose curves for homogeneous phantom, bulk bone, bone with a hole and without the implant, and six different implant materials placed into the bone for (a) 6 MeV and for (b) 9 MeV

Removing an implant from the jaw creates a hole in the bone, and in this study, it is known as Bone Without Implant (BWI). The dose in this area was likely the same for bone and BWI. For the bone area directly in front of the implant, the highest increasing dose occurred for the ZrO$_2$ and Y-TZP implants. Compared to the phantom and the bone, the dose was almost 114.44% and 46.32% higher, respectively. The lowest increasing dose occurred for the PEEK implants (104.85% and 36.73% compared to phantom and bone, respectively). The dose in this area

Table 2. The quantitative data of percentage depth dose at 6 MeV electron beam for different cases in the four important regions

Region	Phantom	Bone	Bone with implant hole	Ti-alloy	Ti	Y-TZP	Al$_2$O$_3$	ZrO$_2$	PEEK
Soft tissue area just in front of the bone (0.9 cm)	95.41	97.54	97.57	99.15	99.23	99.32	98.88	99.33	98.78
The bone area directly in front of the implant (1.25 cm)	99.44	167.56	166.91	210.60	210.02	213.76	206.06	213.88	204.29
The bone area directly behind the implant (1.75 cm)	91.12	93.73	103.23	58.60	58	53.59	62.50	54.14	92.00
Soft tissue area just behind the bone (2.1 cm)	73.08	29.00	31.81	16.85	16.78	16.00	17.15	16.50	22.99

was likely the same for the bone and the BWI. For the bone area directly behind the implant, there was an increased dose in the BWI case (12.11% and 9.5% compared to the phantom and the bone, respectively). The implants' highest and lowest dose reductions were obtained for the Y-TZP and the PEEK, respectively. For the soft tissue area just behind the bone, the highest dose reduction was obtained for the Y-TZP implant (57.08% and 13% compared to the phantom and the bone, respectively).

For 9 MeV and the soft tissue area just in front of the bone, the results are almost the same in all cases (up to 3.25% difference). For the bone area directly in front of the implant; the highest increasing dose occurred for the ZrO_2 and the Y-TZP implant. Compared to the phantom and bone, the dose was almost 108.69% and 44.51% higher. The lowest increasing dose occurred for the PEEK implants (98.84% and 34.66% compared to the phantom and the bone, respectively). The dose in this area was likely the same for the bone and the BWI. For the bone area directly behind the implant, there was an increased

dose in the BWI case (66.68% and 0.98% compared to the phantom and the bone, respectively). The implants' highest and lowest dose reductions were obtained for the Y-TZP and the PEEK, respectively. For the soft tissue area just behind the bone, the highest dose reduction was obtained for the ZrO_2 implant (32.9% and 24.16% compared to the phantom and the bone, respectively).

3.2.2. Dose Profile Curves

Figure 5 shows the dose distribution exactly behind and in front of the bone with and without implants for both energies used. Phantom and BWI were also used to compare profiles-dose. For the 6 MeV energy, the dose reduction behind the bone was obtained on the profile dose curve. 60.2%, 84.36%, and 70.94% were evaluated for BWI, Y-TZP, and PEEK compared to the phantom, respectively. 6.28% and 18.36% were assessed for BWI and Y-TZP compared to the bone, respectively, but there was an increased dose in the dosage profile for PEEK compared with the bone (4.52%). There was not much change in the profile dose curve in front of the bone.

Table 3. The quantitative data of percentage depth dose at 9 MeV electron beam for different cases in the four important regions

| Region	Phantom	Bone	BWI	Ti-alloy	Ti	Y-TZP	Al_2O_3	ZrO_2	PEEK
Soft tissue area just in front of the bone (0.9 cm)	89.49	90.56	90.53	92.14	92.16	92.74	91.51	92.71	91.38
The bone area directly in front of the implant (1.25 cm)	89.46	153.64	153.42	193.71	194.04	198.06	189.15	198.15	188.30
The bone area directly behind the implant (1.75 cm)	96.29	161.93	162.91	153.64	151.13	130.07	165.24	132.55	180.87
Soft tissue area just behind the bone (2.1 cm)	99.26	90.52	92.70	72.02	71.40	65.74	76.15	66.36	85.04
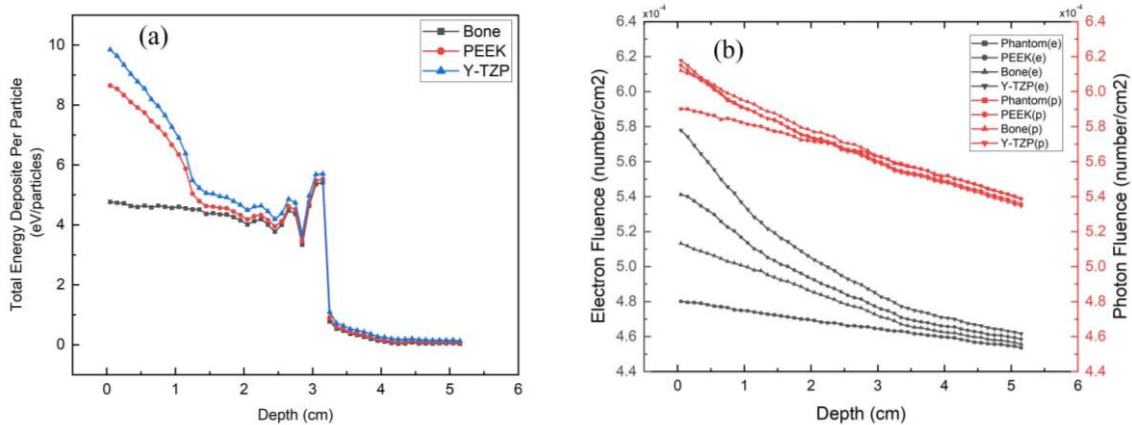
Figure 4. (a) Comparison of the precisely calculated PDD curves for bone, PEEK, and Y-TZP without the phantom energy deposit effect from the distance in front of the implant. (b) Comparison of the photon and electron fluence curves for phantom, bone, PEEK, and Y-TZP from the distance in front of the implant
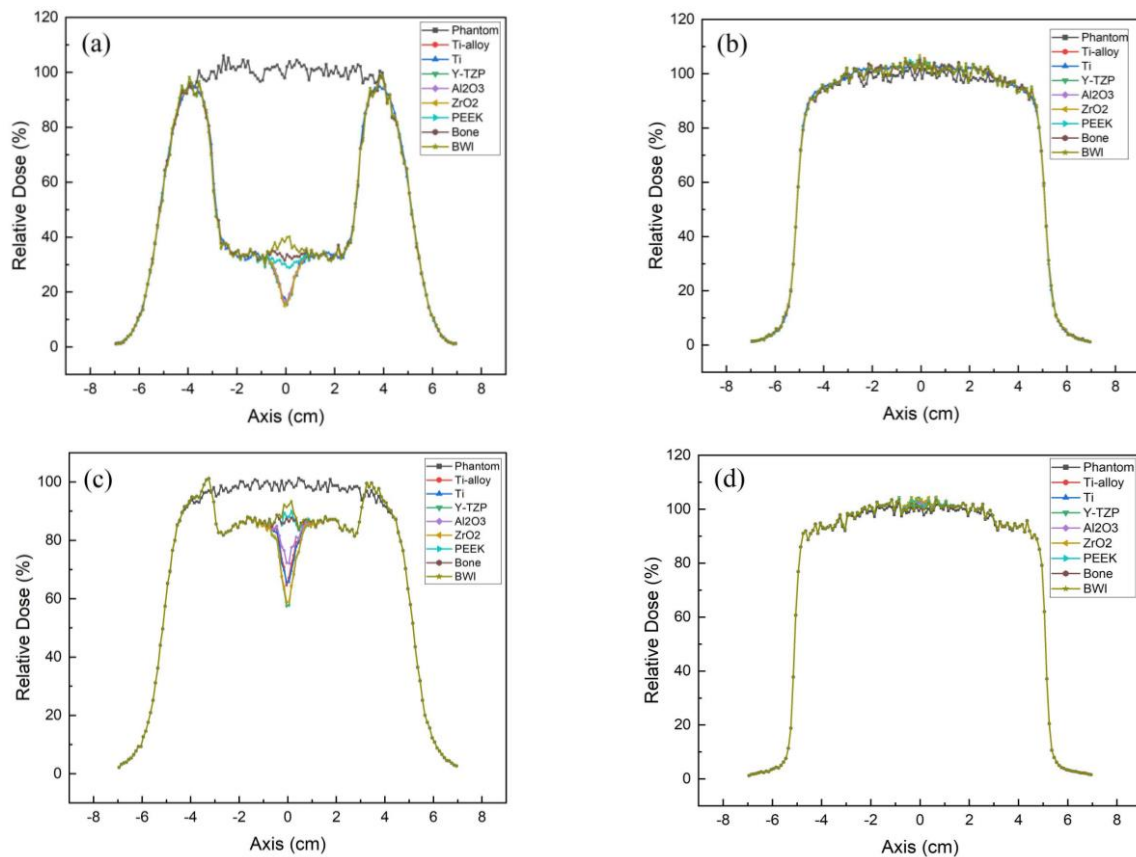
Figure 5. Comparison of the percentage dose profile curves for phantom, bone, BWI, and six different implant materials placed into the bone. The percentage dose profile curves (a) behind the implant position (0.9 cm) at 6 MeV energy, (b) in front of the implant position (2.1 cm) at 6 MeV energy, (c) behind the implant position (0.9 cm) at 9 MeV energy, and (d) in front of the implant position (2.1 cm) at 9 MeV energy. All the profile doses were normalized to the center of axis dose (CAX) of the homogenous phantom

For the 9 MeV energy, the dose reduction dose behind the bone was obtained on the profile dose curve. 8.28%, 12.01%, and 42.26% were evaluated for BWI, Y-TZP, and PEEK compared to the phantom, respectively. 5.64% and 28.73% were assessed for BWI and Y-TZP compared to the bone, respectively, but there was an increased dose in the dosage profile for PEEK compared to the bone (1.52%). There was a slight increase in the profile dose curve in front of the bone (Figure 5d). Figure 6 had a better view of dose increasing and distributing in the bone-phantom interfaces region (Figure 6a) and implant-bone interfaces regions (Figure 6b) on 2D profiles. These interface regions contain 2 different depths behind (Figure 6a, b) and in front (Figure 6a, b) of the bone and implant positions. The homogeneous phantom 2D profiles (Figure 6a, b) are shown in the same depths for better comparison.

4. Discussion

Electrons interact with atoms by different processes due to Coulomb force interactions as they pass through a substance. Two significant processes are inelastic collisions with atomic nuclei (bremsstrahlung) and elastic collisions with atomic electrons (electron-electron scattering), and with atomic nuclei (nuclear scattering). In inelastic collisions, some kinetic energy is changed to other types of energy, such as bremsstrahlung photons. This process is related to the electron energy and the square of the atomic number ($Z2$). Therefore, bremsstrahlung photons are more efficient for higher-energy electrons and higher-atomic-number absorbers. In the elastic collisions with atomic electrons, the high-energy electrons produce multiple small-angle deflections owing to Coulomb force interactions between the incident electrons and the nuclei or electrons of the medium. Therefore, high-energy electrons were scattered from their original direction of motion [23, 24].

This study investigated the effect of different energy, mass density, and atomic numbers on increasing doses in the bone and soft tissue. Two high-density dental implants, Y-TZP and ZrO_2, caused the most increasing dose in the bone and soft tissue for both 6 and 9 MeV energies
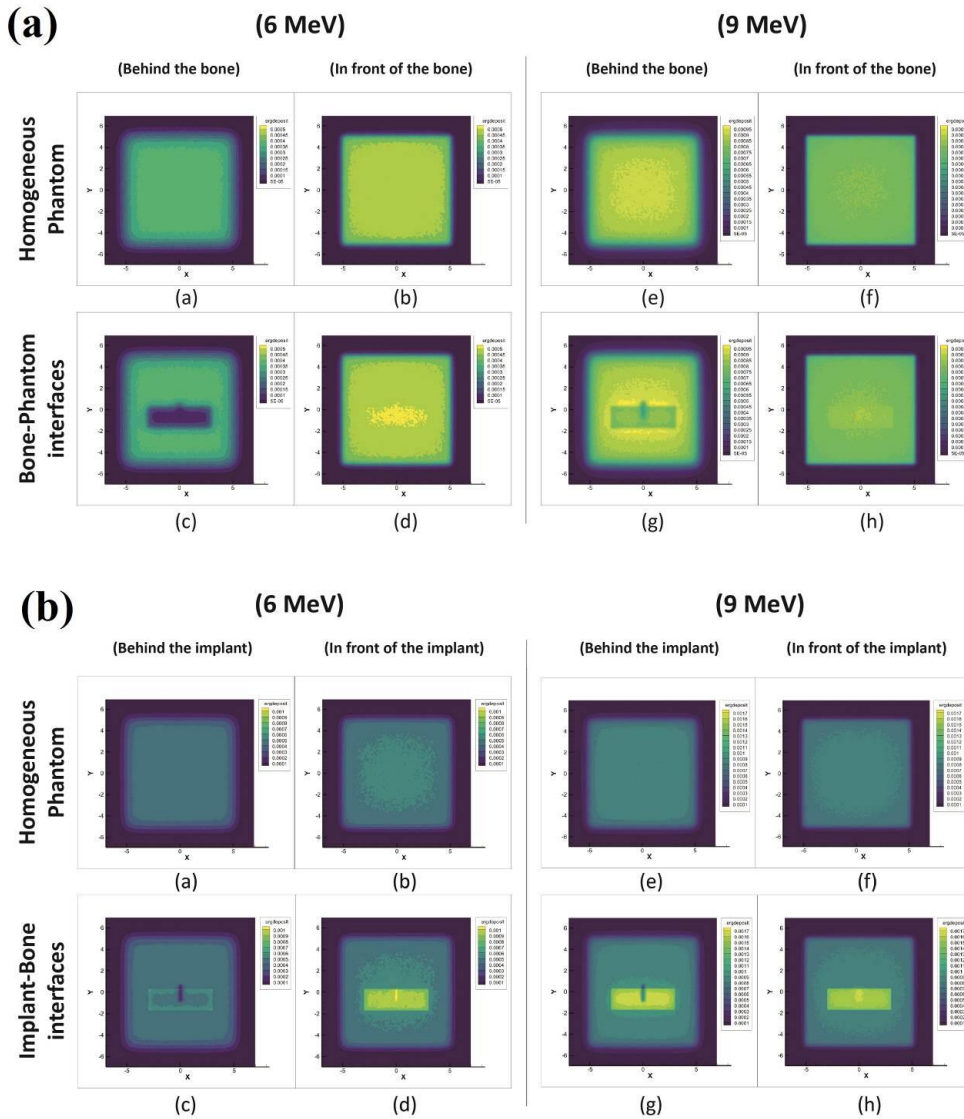
Figure 6. 2D dose profiles in 6 and 9 MeV electron beam energy in (a) bone-phantom interfaces regions and (b) implant-bone interfaces regions

(Figure 3). Figure 4a shows the most increasing dose in the bone due to the highest and the lowest mass density (Y-TZP and PEEK respectively) are approximately 5 eV and 4 eV per transported electron respectively which may cause osteoradionecrosis. The difference in the energy deposit is due to the difference in the scatter electrons fluence (Figure 4b). PEEK is the lowest mass density of dental implants (1.30 g/cm^3), and due to its lower density than adjacent tissue, most electrons pass through the implants without deposition energy. Therefore, the increasing dose behind the depth of PEEK is more than the other implants. The comparison of our study results and other studies is reported in Table 4. Our study investigated the impact of Monte Carlo electron beams on dental implants, specifically focusing on three common materials: Y-TZP, PEEK, and Titanium.

Comparison with existing literature reveals notable variations in percentage dose changes behind and in front of these materials. When examining Y-TZP implants, our results demonstrated a substantial dose reduction of 40.14% behind the implant and an increase of 46.32% in front in 6 MeV. This contrasts with the findings of Akyol *et al.* (2021) [7], where Y-TZP implants showed no significant dose change. Similarly, our study investigated PEEK implants, revealing a dose reduction of 1.73% behind the implant and an increase of 36.73% in front. Comparing these outcomes with Seif *et al.*'s (2018) [25] results, which showed PEEK implants exhibiting a minimal decrease and a more modest increase, further underscores the influence of material properties on radiation effects. These discrepancies may be due to the difference in study conditions, such as the

radiation beam difference in our study, the electron beam was used instead of the photon beam, and the distance difference from the implant interface that dose was measured. Removing an implant from the jaw (known as BWI) can avoid increasing the dose in front of the implant, but this causes an increasing dose behind the implant in both 6 and 9 MeV beams (Figure 3). According to Figure 6, the absolute dose was shown in critical regions as 2D-Profiles. The shadow of bone and implant due

to the attenuation was clearly shown. In addition, dose increasing before implant or bone was shown for both 6 and 9 MeV. As Figure 6 shows, in the behind of bone or implant region, the dose decreasing at the edge of their situation is lower than the central situation (Figure 6c and g). This is because the secondary electrons outside the borders of the bone or implant enter these areas and cause an increase in the dose of these areas.

Table 4. Research features and results pretending to the effects of head and neck radiotherapy and the different dental implant materials and sizes

Study			Beam		Implant features		percentage dose change		Biological effects risks
Name	Study date	Study design	Kind	Energy (MV)	Thickness	Material	Behind implant	In front of the implant	
Khaleghi *et al.*[27]	2021	Measurement	Photon	6	0.4 cm	Ti	-15%	+3-5%	increase
Saadatmand *et al.* [28]	2020	Measurement	Photon	6	Not reported	Amalgam	−6.25%	24.38%	increase
Azizi, *et al.*[29]	2019	Monte Carlo	Photon	15	0.5 cm	Amalgam	−23.50	+3.2%	increase
Reinhard E. Friedrich *et al.* [30]	2010	Monte Carlo	Photon	6	0.4 cm	Ti	-16%	+5%	Increase
Reinhard E. Friedrich *et al* .[4]	2012	Monte Carlo	Photon	6	0.33 cm	Ti	-2.5%	+6%	Increase
Oya Akyol *et al.* [7]	2021	Measurement	Photon	6	0.5 cm	Y-TZP PEEK	- -	2.12 Gy* 1.78 Gy*	Not reported
Oya Akyol *et al.* [26]	2019	Monte Carlo	Photon	6	1cm	Ti Y-TZP PEEK	-15.5% -24.4% -1.1%	+11.2% +20.2% +0.4%	Increase Increase Not affected
Serap Çatli *et al* .[31]	2015	Monte Carlo	Photon	6	1cm	Ti	-14.8%	+7.8%	Debatable
T. Binger *et al.* [32]	2008	Measurement	Photon	6	0.21 cm 0.42 cm	Ti Ti	-8.7% -12.5%	+17.5% +16.3%	Increase
F. Seif *et al* [25].	2018	Monte Carlo	Photon	6	0.4 cm	PEEK Ti-alloy	-2.78% -3.99%	+1% +2.29%	Not reported
This study	-	Monte Carlo	electron	6	0.35 cm	Y-TZP PEEK Ti	-40.14% -1.73% -35.73%	+46.32% +36.73% +42.46%	Increase
				9	0.35 cm	Y-TZP PEEK Ti	-31.86% -18.94% -10.8%	+44.51% +34.66% +40.4%	

* Exact dose-measuring at Gy unit.

One of the most important regions that should be discussed is the bone region directly in front of the implant, which could potentially be at risk of osteoradionecrosis due to the dose increasing in this region due to the backscatter electrons [26]. The Backscatter Factor (BSF) can be utilized for dose correction in treatment planning [7]. It is also a useful measure for comparing the effects of different dental implant materials on dose distribution and increase. In this study, for the 6 and 9 MeV, the Y-TZP has the most effect on BSF (2.15 and 2.21, respectively). The lowest BSF is 2.05 and 2.1 related to PEEK implant for the 6 and 9 MeV, respectively.

5. Conclusion

This study investigated the effect of different energy, mass density, and atomic numbers on increasing doses in the bone and soft tissue. Two high-density dental implants, Y-TZP and ZrO_2, caused the most increasing dose in the bone and soft tissue. The increasing dose behind the soft tissue depth of PEEK is more than the other implants. Removing an implant from the jaw decreases the dose in front of the implant and increases the dose behind the implant.

Acknowledgments

References

1- Rebecca L. Siegel, Kimberly D. Miller, and Ahmedin Jemal, "Cancer statistics, 2019." *CA: A Cancer Journal for Clinicians,* Vol. 69 (No. 1), pp. 7-34, 2019/1// (2019).

2- M. Beyzadeoglu, B. Dirican, K. Oysul, J. Ozen, and O. Ucok, "Evaluation of scatter dose of dental titanium implants exposed to photon beams of different energies and irradiation angles in head and neck radiotherapy." *Dentomaxillofacial Radiology,* Vol. 35 (No. 1), pp. 14-17, 2006/1// (2006).

3- Reham B. Osman and Michael V. Swain, "A Critical Review of Dental Implant Materials with an Emphasis on Titanium versus Zirconia." *Materials,* Vol. 8pp. 932-58, (2015).

4- Reinhard E. Friedrich, Manuel Todorovic, Max Heiland, Hanna A. Scheuer, and Andreas Krüll, "Scattering effects of irradiation on surroundings calculated for a small dental implant." *Anticancer Research,* Vol. 32 (No. 5), pp. 2043-46, (2012).

5- Zeynep Özkurt and Ender Kazazoğlu, "Zirconia Dental Implants: A Literature Review." *Journal of Oral Implantology,* Vol. 37 (No. 3), pp. 367-76, 2011/6// (2011).

6- Andreas Dominik Schwitalla, Tobias Spintig, Ilona Kallage, and Wolf Dieter Müller, "Flexural behavior of PEEK materials for dental application." *Dental Materials,* Vol. 31 (No. 11), pp. 1377-84, 2015/11// (2015).

7- Oya Akyol, Turan Olgar, Turkay Toklu, Hakan Eren, and Bahar Dirican, "Dose distrubution evaluation of different dental implants on a real human dry-skull model for head and neck cancer radiotherapy." *Radiation Physics and Chemistry,* Vol. 189pp. 109751-51, 2021/12// (2021).

8- Bernd Reitemeier *et al.*, "Evaluation of a device for attenuation of electron release from dental restorations in a therapeutic radiation field." *The Journal of Prosthetic Dentistry,* Vol. 87 (No. 3), pp. 323-27, 2002/3// (2002).

9- David W. H. Chin *et al.*, "Effect of dental restorations and prostheses on radiotherapy dose distribution: A monte carlo study." *Journal of Applied Clinical Medical Physics,* Vol. 10 (No. 1), pp. 80-89, (2009).

10- Julide Ozen, Bahar Dirican, Kaan Oysul, Murat Beyzadeoglu, Ozlem Ucok, and Bedri Beydemir, "Dosimetric evaluation of the effect of dental implants in head and neck radiotherapy." *Oral Surgery, Oral Medicine, Oral Pathology, Oral Radiology and Endodontology,* Vol. 99 (No. 6), pp. 743-47, (2005).

11- J. Beumer, R. Harrison, B. Sanders, and M. Kurrasch, "Osteoradionecrosis: predisposing factors and outcomes of therapy." *Head & neck surgery,* Vol. 6 (No. 4), pp. 819-27, (1984).

12- M. M. Curi and L. L. Dib, "Osteoradionecrosis of the jaws: a retrospective study of the background factors and treatment in 104 cases." *Journal of oral and maxillofacial surgery: official journal of the American Association of*

Oral and Maxillofacial Surgeons, Vol. 55 (No. 6), pp. 540-46, 1997/6// (1997).

13- Norah Duv Tapley and G. H. Fletcher, "The Electron Beam in the Treatment of Oral Cavity and Oropharynx Cancer and in 'Boost' Therapy1." Vol. 2, *Electron Beam Therapy: 2nd Annual San Francisco Cancer Symposium, San Francisco, Cal., October 1966: Proceedings*: *S.Karger AG*, (1968), p. 0. [Online]. Available: https://doi.org/10.1159/000426729.

14- Ashutosh Mukherji, "Planning Electron Therapy and Evaluation of Plans." in *Basics of Planning and Management of Patients during Radiation Therapy: A Guide for Students and Practitioners*, Ashutosh Mukherji, Ed. Singapore: *Springer Singapore*, (2018), pp. 209-19.

15- W. Dobrowsky, O. Schlappack, K. H. Kärcher, R. Pavelka, and G. Kment, "Electron beam therapy in treatment of parotid neoplasm." (in eng), *Radiother Oncol,* Vol. 6 (No. 4), pp. 293-9, Aug (1986).

16- C. M. Menard, J. Bews, R. I. Skoracki, and A. D. Chowdhury, "High-energy electron and photon therapy to the parotid bed: radiation dose perturbations with a titanium mandibular implant." *Australas Radiol,* Vol. 43 (No. 4), pp. 495-9, Nov (1999).

17- D. W. O. Rogers and A. F. Bielajew, "Monte Carlo techniques of electron and photon transport for radiation dosimetry." *The dosimetry of ionizing radiation,* Vol. 3pp. 427-539, (1990).

18- Philip von Voigts-Rhetz, Damian Czarnecki, and Klemens Zink, "Effective point of measurement for parallel plate and cylindrical ion chambers in megavoltage electron beams." *Zeitschrift für Medizinische Physik,* Vol. 24 (No. 3), pp. 216-23, 2014/09/01/ (2014).

19- Gregg McKinney, MCNPX User's Manual, Version 2.6.0. (2008).

20- J Kenneth Shultis and Richard E Faw, "An MCNP primer." (2011).

21- Daryoush Sheikh-Bagheri and D. W. O. Rogers, "Sensitivity of megavoltage photon beam Monte Carlo simulations to electron beam and other parameters." *medical physics,* Vol. 29 (No. 3), pp. 379-90, 2002/03/01 (2002).

22- Tsuyoshi Kato, Shinichiro Omachi, and Hirotomo Aso, "Asymmetric gaussian and its application to pattern recognition." *Springer*, pp. 405-13.

23- Faiz M. Khan and John P. Gibbons, Khan's the physics of radiation therapy. 5th editio ed. Philadelphia: *Lippincott Williams & Wilkins*, (2014).

24- Kenneth R. Hogstrom and Peter R. Almond, "Review of electron beam therapy physics." *Physics in Medicine and Biology,* Vol. 51 (No. 13), (2006).

25- F. Seif, T. Seif, M. Athari, M. R. Bayatiyani, and S. Bagheri, "Investigating the effect of dental implants on radiotherapy dose distribution using mont carlo

approach." *Journal of Babol University of Medical Sciences,* Vol. 20 (No. 8), pp. 56-61, (2018).

26- Oya Akyol, Bahar Dirican, Turkay Toklu, Hakan Eren, and Turan Olgar, "Investigating the effect of dental implant materials with different densities on radiotherapy dose distribution using Monte-Carlo simulation and pencil beam convolution algorithm." *Dentomaxillofacial Radiology,* Vol. 48 (No. 4), pp. 20180267-67, 2019/5// (2019).

27- G. Khaleghi *et al.*, "Investigating dose homogeneity in radiotherapy of oral cancers in the presence of a dental implant system: an in vitro phantom study." *Int J Implant Dent,* Vol. 7 (No. 1), p. 90, Sep 6 (2021).

28- P. Saadatmand, A. Amouheidari, A. Shanei, and I. Abedi, "Dose perturbation due to dental amalgam in the head and neck radiotherapy: A phantom study." *Med Dosim,* Vol. 45 (No. 2), pp. 128-33, Summer (2020).

29- M. Azizi, A. A. Mowlavi, M. Ghorbani, C. Knuap, and M. Behmadi, "A Monte Carlo study on dose perturbation due to dental restorations in a 15 MV photon beam." *J Cancer Res Ther,* Vol. 15 (No. 3), pp. 491-97, Jul-Sep (2019).

30- Reinhard E. Friedrich, Todrovic And Manuel, and Krull Andreas, "Simulation of scattering effects of irradiation on surroundings using the example of titanium dental implants: A Monte Carlo approach." *Anticancer Research,* Vol. 30 (No. 5), pp. 1727-30, (2010).

31- Serap Çatli, "High-density dental implants and radiotherapy planning: Evaluation of effects on dose distribution using pencil beam convolution algorithm and Monte Carlo method." *Journal of Applied Clinical Medical Physics,* Vol. 16 (No. 5), pp. 46-52, (2015).

32- Thomas Binger, H. Seifert, G. Blass, K. H. Bormann, and M. Rücker, "Dose inhomogeneities on surfaces of different dental implants during irradiation with high-energy photons." *Dentomaxillofacial Radiology,* Vol. 37 (No. 3), pp. 149-53, (2008).